We are IntechOpen, the world's leading publisher of Open Access books Built by scientists, for scientists

6,900
Open access books available

185,000
International authors and editors

200M
Downloads

Our authors are among the

154
Countries delivered to

TOP 1%
most cited scientists

12.2%
Contributors from top 500 universities



WEB OF SCIENCE™

Selection of our books indexed in the Book Citation Index in Web of Science™ Core Collection (BKCI)

Interested in publishing with us?
Contact book.department@intechopen.com

Numbers displayed above are based on latest data collected.
For more information visit www.intechopen.com



Chapter 2

Acoustic Analysis of Enclosed Sound Space as well as Its Coupling with Flexible Boundary Structure

Jingtao Du, Yang Liu and Long Liu

Additional information is available at the end of the chapter

http://dx.doi.org/10.5772/intechopen.69967

Abstract

Combustion instability is often encountered in various power systems, a good understanding on the sound field in acoustic cavity as well as its coupling with boundary flexible structure will be of great help for the reliability design of such combustion system. An improved Fourier series method is presented for the acoustic/vibro-acoustic modelling of acoustic cavity as well as the panel-cavity coupling system. The structural-acoustic coupling system is described in a unified pattern using the energy principle. With the aim to construct the admissible functions sufficiently smooth for the enclosed sound space as well as the flexible boundary structure, the boundary-smoothed auxiliary functions are introduced to the standard multi-dimensional Fourier series. All the unknown coefficients and higher order variables are determined in conjunction with Rayleigh-Ritz procedure and differential operation term by term. Numerical examples are then presented to show the correctness and effectiveness of the current model. The model is verified through the comparison with those from analytic solution and other approaches. Based on the model established, the influence of boundary conditions on the acoustic and/or vibro-acoustic characteristics of the structural-acoustic coupling system is addressed and investigated.

Keywords: enclosed sound space, acoustics analysis, structural-acoustic coupling, flexible boundary structure

1. Introduction

Combustion instability is often encountered in various power systems, which will further cause the combustion noise or even the dynamic damage of combustion chamber structure [1]. A good understanding on the vibro-acoustic coupling between the bounded flexible structure and the thermo-driven acoustic oscillation will be of great significance for the correct design of combustion system of various power plants. As an important part of such whole thermos-acoustic

INTECH
open science | open minds

© 2017 The Author(s). Licensee InTech. This chapter is distributed under the terms of the Creative Commons Attribution License (http://creativecommons.org/licenses/by/3.0), which permits unrestricted use, distribution, and reproduction in any medium, provided the original work is properly cited. CC BY

coupling system, the acoustics in cavity and its coupling with its flexible boundary also plays an important role. For many years, a lot of research effort has been devoted to the coupled structural-acoustic system.

The acoustic analysis in enclosed space is a classical research topic in acoustics community, and the rectangular cavity is widely used as the theoretical model. Morse and Bolt [2] first introduced the normal modes theory into room acoustics, and developed a non-linear transcendental characteristic equation through combining the assumed sound pressure modes with complex impedance boundary conditions on the walls. Maa [3] derived the transcendental equation for a rectangular room with non-uniform acoustical boundaries which took the same form as that of a uniform acoustic admittance case, while the impedance term was consequently non-uniform on certain wall. Recent studies have been mainly focused on developing more effective root searching algorithms for finding eigensolutions. For instance, Bistafa and Morrissey [4] compared two different numerical procedures: one is the Newton's method and the other is referred to as the homotopic continuation technique based on the numerical integration of differential equations. The roots are searched for the cases from soft walls to the terminal impedance with small increments. They found that the latter procedure is much faster in finding all the possible roots. Naka et al. [5] utilized an interval Newton/generalized bisection (IN/GB) method to find the roots of the non-linear characteristic equation within any given interval for the modal analysis of rectangular room with arbitrary wall impedances.

In many occasions, the acoustic cavity is bounded by the flexible structure, and the interaction between the structural vibration and the acoustic cavity should be taken into account simultaneously for the determination of acoustic field characteristics. Among the existing studies, the most popular modelling approach is the so-called modal coupling theory [6] in which the structural modes *in vacuo* and the acoustic cavity modes with rigid walls need to be determined *a priori*. The two sets of modes are then combined together, via spatial coupling coefficients, to find the response of the coupled system. However, as pointed out by Pan et al. [7, 8], there are two main limitations with the modal coupling theory. One is that such an approach is only suitable for weak coupling and will be inadequate in dealing with strong coupling conditions as in the cases where a very thin plate, a shallow cavity depth or a heavy medium is involved. The other one is related to the use of the rigidly walled cavity modes since then the particle vibrational velocity on contacting surface cannot be determined from the pressure gradient, causing the discontinuity of velocity from the cavity to the vibrational panel. In other words, the basic requirement of velocity continuity on the panel-cavity coupling interface cannot be satisfied by the modal coupling theory. Then, this approach may be problematic when the energy transmission is needed for the analysis, since it will be difficult to calculate the high-order variable using the acoustic mode with rigid wall.

In this chapter, a unified structural-acoustic coupling analysis framework will be introduced for the representative rectangular cavity and its coupled panel structure. The fully coupling system is described in the framework of energy. The Fourier series with supplementary terms is constructed as the admissible functions, which are smoothed in the whole solving domain including the elastic structural and/or impedance acoustic boundary and coupling interface. All the unknown coefficients are solved in conjunction with Rayleigh-Ritz procedure. Since the

field functions are sufficiently smooth, the corresponding high-order variables can be calculated straightforwardly.

2. Theoretical formulations

2.1. Acoustic cavity with impedance boundary condition

A rectangular acoustical cavity of dimensions $L_x \times L_y \times L_z$ and the associated coordinate system are sketched in **Figure 1**. In this study, it is assumed that an arbitrary impedance boundary condition is specified on each of the cavity surfaces, that is,

$$\frac{\partial p}{\partial n} = -j\frac{\rho c}{Z_i}kp \tag{1}$$

where $j = \sqrt{-1}$, p is the sound pressure, n denotes the outgoing normal of the surface, ρ and c are respectively the mass density and the sound speed in the acoustic medium, k (= ω/c) is the wavenumber with ω being angular frequency, and Z_i represents the acoustic impedance on the ith surface.

2.2. Improved Fourier series representation of admissible function

It is well known that the modal functions for rigid-walled rectangular cavity are simply the products of cosine functions in three dimensions. Based on the modal superposition principle, the corresponding sound pressure field inside the cavity can be generally expressed as a 3-D Fourier cosine series. However, such a Fourier series representation will become problematic when an impedance boundary condition is specified on one or more of the interior walls. This assertion is evident from Eq. (1) because the left side of the equation is identically equal to zero regardless of the actual value of the right side. This problem is mathematically related to the inability to converge of the traditional Fourier series on the boundaries of a domain under general boundary conditions. To overcome this difficulty, in this study, a 3-D version of an

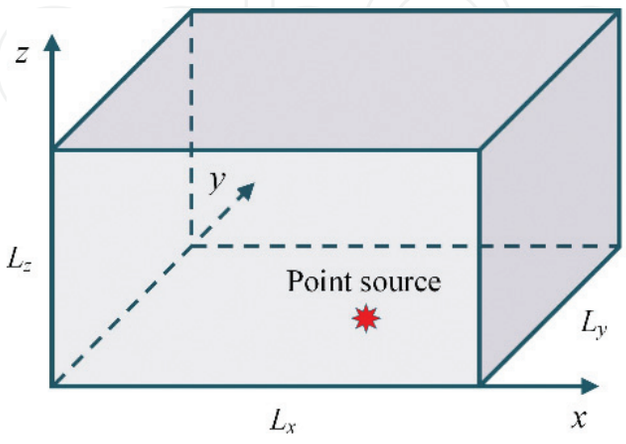


Figure 1. A rectangular cavity with general impedance boundary conditions.

improved Fourier series representation previously developed for the in-plane vibrations of elastically restrained plates will be used to expand the sound pressure inside the cavity [9].

$$\begin{aligned} p(x,y,z) = &\sum_{m_x=0}^{\infty}\sum_{m_y=0}^{\infty}\sum_{m_z=0}^{\infty} A_{m_x m_y m_z}\cos\lambda_{m_x}x\cos\lambda_{m_y}y\cos\lambda_{m_z}z \\ &+\sum_{m_x=0}^{\infty}\sum_{m_y=0}^{\infty}\left[\underbrace{\xi_{1L_z}(z)a_{m_x m_y}}_{z=0}+\underbrace{\xi_{2L_z}(z)b_{m_x m_y}}_{z=L_z}\right]\cos\lambda_{m_x}x\cos\lambda_{m_y}y \\ &+\sum_{m_x=0}^{\infty}\sum_{m_z=0}^{\infty}\left[\underbrace{\xi_{1L_y}(y)c_{m_x m_z}}_{y=0}+\underbrace{\xi_{2L_y}(y)d_{m_x m_z}}_{y=L_y}\right]\cos\lambda_{m_x}x\cos\lambda_{m_z}z \\ &+\sum_{m_y=0}^{\infty}\sum_{m_z=0}^{\infty}\left[\underbrace{\xi_{1L_x}(x)e_{m_y m_z}}_{x=0}+\underbrace{\xi_{2L_x}(x)f_{m_y m_z}}_{x=L_x}\right]\cos\lambda_{m_y}y\cos\lambda_{m_z}z \end{aligned} \tag{2}$$

where $\lambda_{ms} = m_s\pi/L_s$, ($s = x, y$ or z), and the supplemental functions are defined as

$$\xi_{1L_s}(s) = L_s\zeta_s(\zeta_s-1)^2,\ \xi_{2L_s}(s) = L_s\zeta_s^2(\zeta_s-1),\ (\zeta_s = s/L_s) \tag{3}$$

It is easy to verify that

$$\xi_{1L_s}(0) = \xi_{1L_s}(L_s) = \xi'_{1L_s}(L_s) = 0,\ \xi'_{1L_s}(0) = 1 \tag{4}$$

$$\xi_{2L_s}(0) = \xi_{2L_s}(L_s) = \xi'_{2L_s}(0) = 0,\ \xi'_{2L_s}(L_s) = 1 \tag{5}$$

In light of Eqs. (3)–(5), one can understand that the 2-D Fourier series expansions in Eq. (2) mathematically represent the possible non-zero (normal) derivatives of the acoustic pressure on each of the cavity walls, and the 3-D Fourier series a residual pressure field as if the impedance boundary conditions on the cavity walls were modified to being infinite rigid. Mathematically, it can be proved that the modified series solution converges faster and uniformly over the entire solution domain including the boundary walls [10, 11].

Since the pressure solution is constructed sufficiently smooth in the current formulation, the unknown expansion coefficients can be solved in a strong form by letting the series solution simultaneously satisfy both the governing differential equation (Helmholtz equation) inside the cavity and the boundary conditions, on the cavity walls on a point-wise basis. In such a case, because of the boundary conditions, the expansion coefficients for the 2-D series are not fully independent of those for the 3-D series. While such a procedure may be preferred in the context of 'exact' solution, an alternative procedure for obtaining a weak form of solution will be employed here because of its potential benefits in modelling complex acoustic systems consisting of many cavities. The corresponding Lagrangian for the rectangular cavity with arbitrary impedance boundary conditions can be written as

$$L = V - T - W_{ext} \tag{6}$$

where V denotes the total acoustic potential energy stored in the enclosed volume, T represents the total kinetic energy and W_{ext} represents all the work done by the applied sources which include the energy dissipation on the wall surfaces in the current case. These terms can be explicitly expressed as [12].

The total potential energy V is

$$V = \frac{1}{2\rho_0 c_0^2}\int_V p^2 dV = \frac{1}{2\rho_0 c_0^2}\int_0^{L_x}\int_0^{L_y}\int_0^{L_z} p^2(x,y,z)dxdydz \tag{7}$$

where c_0 is the speed of sound, and ρ_0 is the mass density of the medium in the cavity.

The total kinetic energy T is given as

$$\begin{aligned} T &= \frac{1}{2\rho_0\omega^2}\int_V (\text{grad } p)^2 dV \\ &= \frac{1}{2\rho_0\omega^2}\int_V \left[\left(\frac{\partial p}{\partial x}\right)^2 + \left(\frac{\partial p}{\partial y}\right)^2 + \left(\frac{\partial p}{\partial z}\right)^2\right] dV \\ &= \frac{1}{2\rho_0\omega^2}\int_0^{L_x}\int_0^{L_y}\int_0^{L_z} \left[\left(\frac{\partial p}{\partial x}\right)^2 + \left(\frac{\partial p}{\partial y}\right)^2 + \left(\frac{\partial p}{\partial z}\right)^2\right] dxdydz \end{aligned} \tag{8}$$

where grad p means the gradient of sound pressure.

By using the relationship between the sound pressure and the particle velocity on impedance surface, the dissipated acoustic energy can be calculated from

$$W_{wall} = -\frac{1}{2}\int_S \frac{p^2}{j\omega}\frac{1}{Z}dS = -\frac{1}{2}\int_S \frac{p^2}{j\omega}\Upsilon dS \tag{9}$$

where Z is the complex acoustic impedance of the wall surface, and Υ is the complex acoustic admittance which is defined as the inverse of impedance, namely, $\Upsilon = 1/Z$. For the non-uniform distributed on a wall surface to account for practical complications, for example, the acoustic admittance on wall $z = 0$ can be generally described as $\Upsilon_{z0}(x, y) = \Upsilon_A \times h_{z0}(x, y)$ where Υ_A is the complex amplitude and $h_{z0}(x, y)$ is a strength distribution function. In this study, to unify the formulations and simplify the subsequent calculations, any specified admittance distribution, such as $\Upsilon_{z0}(x, y)$, will be expanded into double Fourier series as

$$\Upsilon_{x0}(y,z) = \sum_{n_y=0}^{\infty}\sum_{n_z=0}^{\infty} \tilde{\Upsilon}_{x0}^{n_y n_z} \cos\lambda_{n_y} y \cos\lambda_{n_z} z \tag{10}$$

where $\lambda_{ns} = n_s\pi/L_s$, ($s = y$ or z). In actual numerical calculations, all such Fourier series expansions will be truncated to $n_y = N_y$ and $n_y = N_z$. The non-uniform impedance distributions on other wall surfaces can be treated in the same way.

The work done by a sound source inside cavity can be represented as

$$W_S = -\frac{1}{2}\int_V \frac{pQ}{j\omega} dv \tag{11}$$

where Q is the distribution function of a sound source. For a point source located at (x_e, y_e, z_e) inside the cavity, we have

$$Q = Q_0\delta(x - x_e)\delta(y - y_e)\delta(z - z_e) \tag{12}$$

where Q_0 is the volume velocity amplitude of the sound source, and δ is Dirac delta function.

Substituting Eqs. (7)–(12) into the acoustic Lagrangian, Eq. (6), and applying the Rayleigh-Ritz procedure against each of the unknown Fourier series coefficient, a system of linear algebra equations can be derived as

$$(\mathbf{K} + \omega\mathbf{Z} + \omega^2\mathbf{M})\mathbf{E} = \mathbf{Q} \tag{13}$$

where **K** and **M** are the stiffness and mass matrixes of the acoustic system, respectively; **Z** is the damping matrix due to the dissipative effect of the impedance boundary conditions over the cavity walls and **Q** is the external load vector.

In order to determine the modal characteristics of the acoustic cavity, one needs to solve the characteristic equation by setting the external load vector **Q** (on the right side of Eq. (14)) to zero. Since the resulting equation will involve the first-order and second-order terms of oscillation frequency, it is usually rewritten in state space form [13]

$$(\mathbf{R} - \omega\mathbf{S})\mathbf{G} = \mathbf{0} \tag{14}$$

where $\mathbf{R} = -\begin{bmatrix} [\mathbf{0}] & \mathbf{K} \\ \mathbf{K} & \mathbf{Z} \end{bmatrix}$, $\mathbf{S} = \begin{bmatrix} -\mathbf{K} & [\mathbf{0}] \\ [\mathbf{0}] & \mathbf{M} \end{bmatrix}$, $\mathbf{G} = \begin{Bmatrix} \mathbf{E} \\ \mathbf{F} \end{Bmatrix}$ and $\mathbf{F} = \omega\mathbf{E}$.

2.3. Vibro-acoustic coupling of panel-cavity system

The above formulation is mainly about the modelling of pure acoustic cavity, in many situations, the cavity is bounded by the flexible structure, such as the combustion chamber. For such structural-acoustic coupling system, the vibration of flexible boundary structure and the acoustic filed will couple together. As a classical example, the rectangular panel-cavity is often used as the analysis example for the structural-acoustic coupling study.

As shown in **Figure 2**, an elastically restrained plate is one of the surfaces enclosing a rectangular acoustical cavity (other five surfaces are assumed to be perfectly rigid for simplicity). Suppose that the plate is excited by a normal concentrated force F. The vibration of the plate will cause sound waves radiated into the cavity, and the cavity will in turn affect the panel vibration by applying sound pressure to the fluid-structure interface. While the phenomenon is described as causal event, it actually defines a coupled structure-acoustical system in which the two different physical processes affect each other and have to be determined simultaneously by considering the coupling conditions at the interface.

http://dx.doi.org/10.5772/intechopen.69967

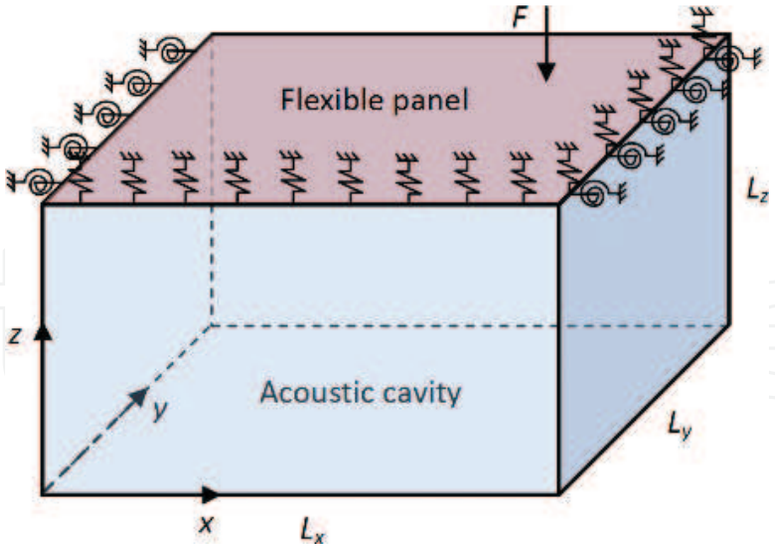


Figure 2. A rectangular acoustic cavity bounded by a flexible panel with general boundary conditions.

Although such structural-acoustic coupling system can be analysed by solving the governing equation and boundary conditions, simultaneously. Similar to the above acoustic analysis of enclosed sound space, the energy principle can also give the sufficiently accurate prediction of vibro-acoustic behaviour, when the admissible functions are constructed smooth enough. For the transverse vibration of a rectangular plate with general elastic boundary supports, its displacement function will be invariantly expanded into an improved Fourier series as [14].

$$w(x,y) = \sum_{m=0}^{\infty}\sum_{n=0}^{\infty} A_{mn}^{p} \cos\lambda_{L_x m}x \cos\lambda_{L_y n}y + \sum_{l=1}^{4}\left(\zeta_{lL_y}(y)\sum_{m=0}^{\infty} c_m^l \cos\lambda_{L_x m}x + \zeta_{lL_x}(x)\sum_{n=0}^{\infty} d_n^l \cos\lambda_{L_y n}y\right) \tag{15}$$

where $\lambda_{Lxm} = m\pi/L_x$, $\lambda_{Lyn} = n\pi/L_y$ and the superscript p with A_{mn} means the Fourier coefficients for the panel displacement. The supplementary functions $\zeta_{lLx}(x)$ and $\zeta_{lLy}(y)$ are introduced to account for all the possible discontinuities with the first and third partial derivatives (with respect to x or y) of the displacement function along each edge of the plate.

For the panel cavity considered here, the main attention will be paid to the structural-acoustic continuity, with the other walls kept as rigid. The acoustic pressure filed function is constructed as [15]

$$\begin{aligned} p(x,y,z) = &\sum_{m_x=0}^{\infty}\sum_{m_y=0}^{\infty}\sum_{m_z=0}^{\infty} A_{m_x m_y m_z}^{a} \cos\lambda_{m_x}x \cos\lambda_{m_y}y \cos\lambda_{m_z}z \\ &+ \xi_{2L_z}(z)\sum_{m_x=0}^{\infty}\sum_{m_y=0}^{\infty} b_{m_x m_y}^{a} \cos\lambda_{m_x}x \cos\lambda_{m_y}y \end{aligned} \tag{16}$$

where m_x, m_y and m_z are all integers, describing the spatial characteristic of a particular mode, $Am_xm_ym_z$ is the complex modal amplitude corresponding to the (m_x, m_y, m_z) mode, and $\lambda_{ms} = m_s\pi/L_s$ $(s = x, y \text{ or } z)$.

The Lagrangian for the plate structure can be expressed as

$$L_{panel} = U_{panel} - T_{panel} - W_{panel} + W_{a\&p} \tag{17}$$

where U_{panel} is the total potential energy associated with the transverse deformation of the panel and the potential energy stored in the restraining springs; T_{panel} denotes the total kinetic energy of the plate; W_{panel} is the work done by the external force F; and $W_{a\&p}$ represents the work done by the sound pressure acting on the structural-acoustic interface which is calculated from

$$W_{a\&p} = \int_S wpdS = \int_0^{L_x}\int_0^{L_y} wpdxdy \tag{18}$$

The total potential and kinetic energy for the elastic plate can be explicitly expressed as

$$\begin{aligned} U_{panel} =& \frac{D}{2}\int_0^{L_x}\int_0^{L_y}\left\{\left(\frac{\partial^2 w}{\partial x^2}\right)^2 + \left(\frac{\partial^2 w}{\partial y^2}\right)^2 + 2\mu\frac{\partial^2 w}{\partial x^2}\frac{\partial^2 w}{\partial y^2} + 2(1-\mu)\left(\frac{\partial^2 w}{\partial x \partial y}\right)^2\right\}dxdy \\ &+ \frac{1}{2}\int_0^{L_y}\left[k_{x0}w^2 + K_{x0}\left(\frac{\partial w}{\partial x}\right)^2\right]_{x=0} dy + \frac{1}{2}\int_0^{L_y}\left[k_{xL_x}w^2 + K_{xL_x}\left(\frac{\partial w}{\partial x}\right)^2\right]_{x=L_x} dy \\ &+ \frac{1}{2}\int_0^{L_x}\left[k_{y0}w^2 + K_{y0}\left(\frac{\partial w}{\partial y}\right)^2\right]_{y=0} dx + \frac{1}{2}\int_0^{L_y}\left[k_{yL_y}w^2 + K_{yL_y}\left(\frac{\partial w}{\partial y}\right)^2\right]_{y=L_y} dx \end{aligned} \tag{19}$$

and

$$T_{panel} = \frac{1}{2}\int_0^{L_x}\int_0^{L_y}\rho h\left(\frac{\partial w}{\partial t}\right)^2 dxdy = \frac{1}{2}\rho h\omega^2\int_0^{L_x}\int_0^{L_y} w^2 dxdy \tag{20}$$

where ρ and h are the mass density and thickness of the plate structure, respectively.

The Lagrangian for the acoustic cavity is

$$L_{cavity} = U_{cavity} - T_{cavity} - W_{p\&a} \tag{21}$$

where U_{cavity} is the total potential energy for the acoustic cavity, T_{cavity} is the total kinetic energy of the particle vibrations inside the cavity and $W_{p\&a}$ denotes the work due to the panel vibration. The (pressure and velocity) continuity conditions the solid-fluid interface implies a reciprocity relationship, that is, $W_{p\&a} = W_{a\&p}$.

Substituting Eqs. (15) and (16) into Eqs. (17) and (21) and minimizing them against the unknown Fourier coefficients, one is able to obtain the final system in matrix form as

$$\left\{\begin{bmatrix} \mathbf{K_p} & \mathbf{C_{a\&p}} \\ \mathbf{0} & \mathbf{K_a} \end{bmatrix} - \omega^2\begin{bmatrix} \mathbf{M_p} & \mathbf{0} \\ -\mathbf{C}_{\mathbf{a\&p}}^T & \mathbf{M_a} \end{bmatrix}\right\}\begin{bmatrix} \mathbf{W} \\ \mathbf{P} \end{bmatrix} = \begin{Bmatrix} \mathbf{F_p} \\ \mathbf{0} \end{Bmatrix} \tag{22}$$

http://dx.doi.org/10.5772/intechopen.69967

Once the Fourier coefficient vectors **W** and **P** are solved from Eq. (22), the structural displacement on the plate and the sound pressure in the cavity can be readily determined by using Eqs. (15) and (18). If one is only interested in the modal parameters of the coupled structural-acoustic system, they can be simply obtained from solving a standard matrix characteristic equation by setting to zero the loading vector on right hand side of Eq. (22), instead of searching the singularities (the poles) of the modal coefficients or extracting the resonant peaks from the frequency response functions of the coupled system. It should be noted that although only one of cavity surfaces is considered movable in the above discussion, the present method can be readily extended to an acoustic cavity bounded by multiple plate structures.

3. Numerical examples and discussion

In this section, numerical examples will be presented to demonstrate the effectiveness and reliability of the proposed method, then based on model established, the vibro-acoustic behaviour of the cavity as well as its coupling system with the flexible panel will be studied. The first example involves a rectangular cavity with each of its walls being perfectly rigid. The related parameters are as follows: the dimensions are $L_x \times L_y \times L_z = 0.7 \times 0.6 \times 0.5\ \mathrm{m}^3$, the air density is ρ_{air} = 1.21 kg/m^3 and the speed of sound is c_0.= 340 m/s. For a non-dissipative wall, its acoustic impedance is described only by an imaginary part.

Table 1 shows a comparison of the first six natural frequencies using the familiar analytic solution and from the current method. It should be mentioned that the current results were calculated by truncating the series expansions in Eq. (2) to $M_x = M_y = M_z = 3$. The 'perfect' match between the current results and the exact solution partially indicates the excellent mathematical characteristic of the proposed series solution in terms of its convergence and accuracy. Although only the first six modes were compared in **Table 1**, a nice agreement for other higher order modes is also evident from the acoustic response curves presented in **Figure 3**. In the subsequent calculations, all the Fourier series expansions will be truncated to $M = 3$ in each direction unless otherwise specified.

Now, place a point source of strength $Q_0 = 2 \times 10^{-5}\ \mathrm{m}^3/\mathrm{s}$ into the acoustic cavity at position (L_x/10, L_y/10 and L_z/10). To account for the air absorption, a modal damping ratio $\eta = 0.01$ is assumed for each acoustic mode. For a relatively small acoustic damping ratio, the dissipative effect can be accounted for simply through introducing a complex wavenumber $k' = k(1 - j\xi)$ [16]. In this

	Natural frequency (Hz)					
	1	**2**	**3**	**4**	**5**	**6**
Current	0.00	242.86	283.33	340.00	373.17	417.83
Analytical	0.00	242.86	283.33	340.00	373.17	417.83

Table 1. The six lowest natural frequencies for a cavity with perfectly rigid walls.

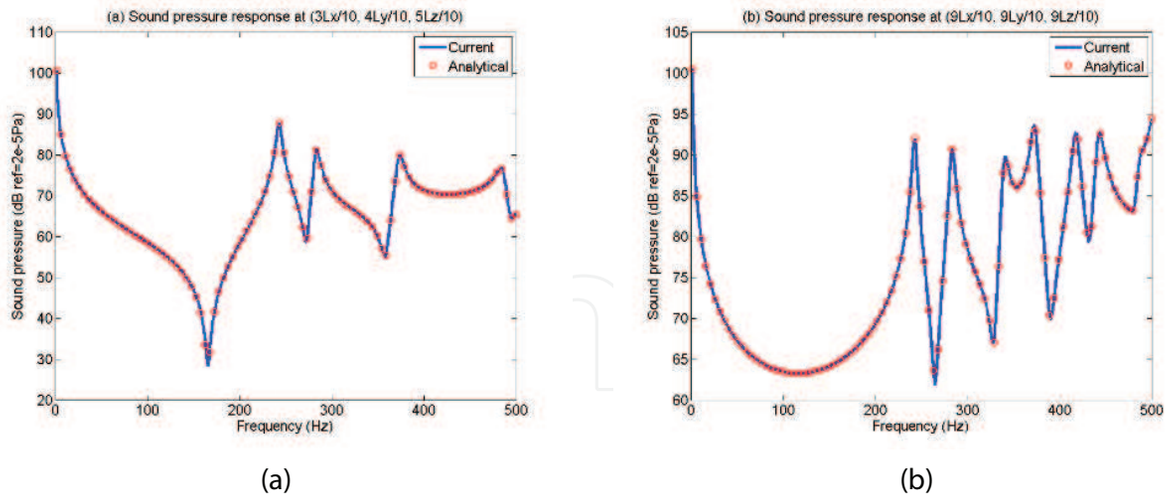


Figure 3. Sound pressure responses inside the cavity at: (a) ($3L_x/10$, $4L_y/10$, $5L_z/10$) and (b) ($9L_x/10$, $9L_y/10$, $9L_z/10$).

method, a complex sound speed $\tilde{c} = c(1 - j\eta)$ is used instead. Since $k' = \omega/\tilde{c}$ (or, $\omega/[c(1 - j\eta)] = k(1 - j\xi)$), it is easy to see that $\eta = -\xi/(1 - j\xi)$. The sound pressure levels at two observation points, ($3L_x/10$, $4L_y/10$, $5L_z/10$) and ($9L_x/10$, $9L_y/10$, $9L_z/10$), are plotted in **Figure 3** in the frequency range of 0–500 Hz. For comparison, the results obtained based on the superposition of 245 analytical modes are also presented. An excellent comparison between the two predictions is seen over the entire frequency range [16].

Another extreme case of the non-dissipative boundary conditions is the so-called pressure release (or zero-pressure), which is described by infinitely small pure imaginary impedance on surface ($j10^{-5}$ in the actual calculations). Suppose that a cavity of $2.12 \times 6.06 \times 2.12$ m^3 has a pressure-release condition at surface $y = L_y$ (= 6.06 m), and the rest walls are perfectly rigid. A point source with strength as $Q_0 = 2 \times 10^{-5}$ m^3/s is placed at (1.86, 0.26 and 0.26 m). To account for the larger dimension in the y direction, more expansion terms are retained accordingly, that is, $M_y = 7$ as compared with $M_x = M_z = 3$.

The sound pressure at (0.1, 5.96 and 2.02 m) is plotted in **Figure 4** as a function of frequency. This problem was previously solved by using an equivalent source technique, and the result was also shown in **Figure 4** as a reference. It is seen that the two predictions are in a good agreement. However, slight separation between them can be noticed as frequency increases. This is probably caused by the possible loss of the accuracy of the equivalent source technique due to the use of an insufficient number of equivalent sources at higher frequencies. Plotted in **Figure 5** are sound pressure fields inside the cavity at 14 and 42 Hz, respectively. Since two frequencies are very close to the first two resonance frequencies (refer to **Figure 4**), the distributions essentially resemble the first and second acoustic mode shapes. It is observed from **Figure 5** that the sound pressure decreases rapidly in approaching to (and eventually vanishes on) the wall of $y = L_y$. The pressure fields are basically uniform on the cross-section perpendicular to y-axis. These two pressure patterns may be considered to evolve the familiar (1, 0, 0) and (2, 0, 0) modes for the cavity with each wall being perfectly rigid. The existence of the zero-pressure wall at $y = L_y$ causes the nodal surfaces to shift towards it.

http://dx.doi.org/10.5772/intechopen.69967

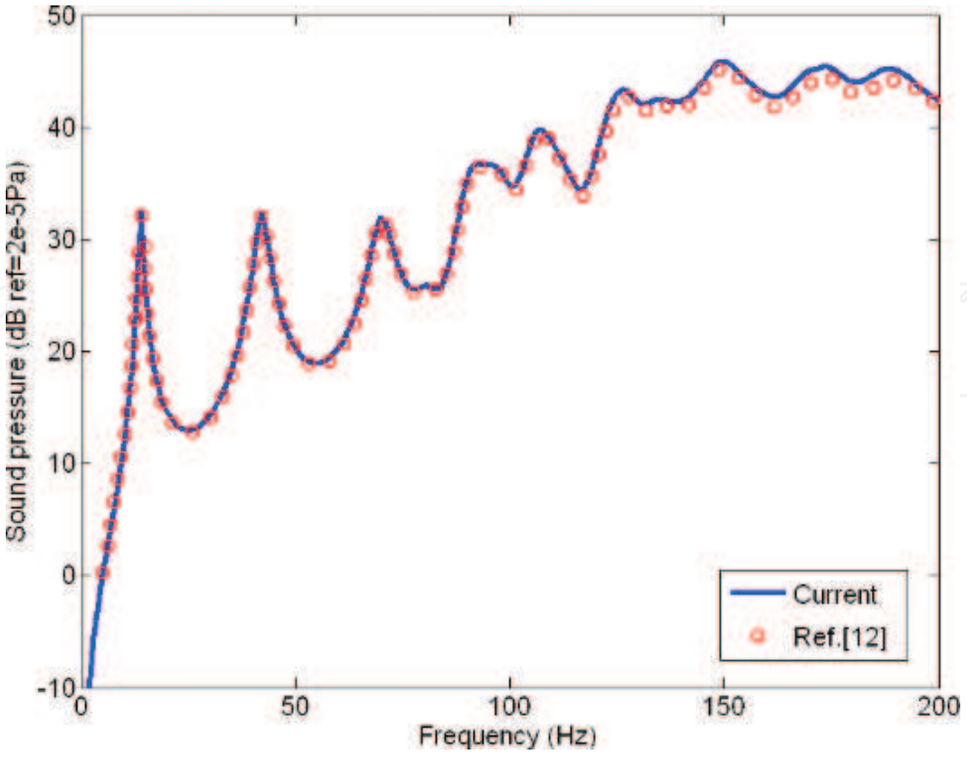


Figure 4. Sound pressure at (0.1, 5.96 and 2.02 m) inside the cavity with pressure release boundary specified on the wall $y = L_y$.

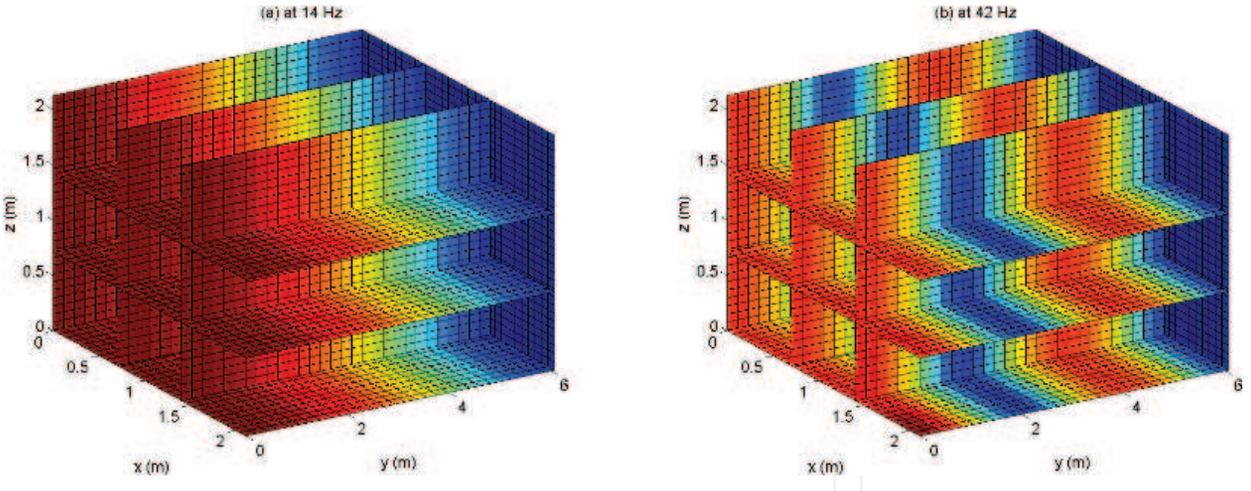


Figure 5. Sound pressure fields with a pressure release described by an infinitely small impedance on the surface ($j10^{-5}$ in the actual calculations) on surface $y = L_y$ (=6.06m) at: (a) 14 Hz and (b) 42 Hz.

To better understand the effect of impedance boundary conditions on the acoustical characteristic of an enclosed space, the frequency responses at the observing point (0.1, 5.96 and 2.02 m) are plotted in **Figure 6** for a wide range of impedance values from $j10^{-5}$ to $j10^{5}$ specified on surface $y = L_y$ (= 6.06 m), while the other walls are kept acoustically rigid. For small impedances, $Z_i \leq j10^{4}$, both the resonance frequencies and response amplitudes show a strong

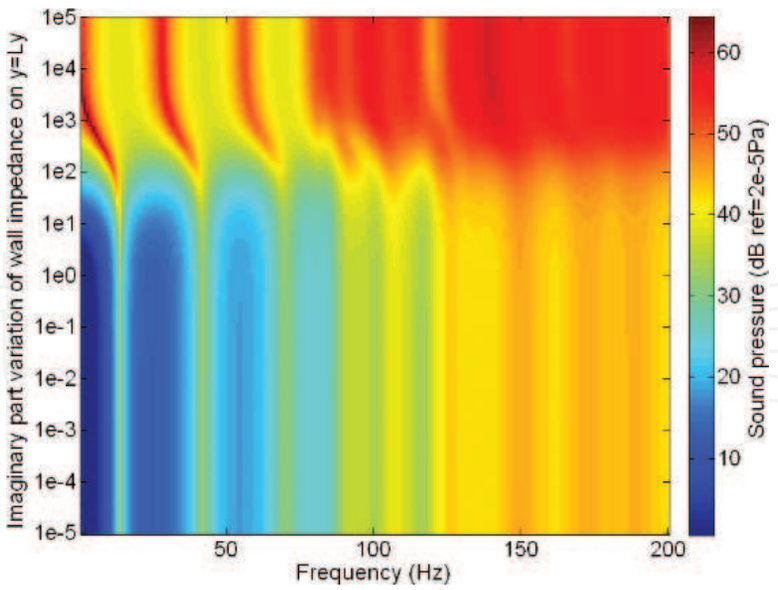


Figure 6. Effect of varying impedance boundary condition on the sound pressure response at observing position (0.1, 5.96 and 2.02 m), in which the impedance variation is specified on surface $y = L_y$ (=6.06 m) while the other walls are kept acoustically rigid.

dependence on the specified impedance value. However, when the wall becomes sufficiently rigid, $Z_i > j10^4$, a further increase of the impedance will have little effect on the pressure field.

In the aforementioned examples, the results are mainly on the acoustic cavity analysis, as demonstrated in the above formulations, the current modelling framework can be used for the treatment of vibro-acoustics analysis of panel-cavity system by simply including the vibrational energy in the whole description. The model will be first valeted, and then, the main emphasis will be put on the model validation and the influence of structural boundary condition on the coupling characteristics of such panel-cavity system.

For the model verification on the modal parameter prediction, consider a problem previously studied in Ref. [17] where an acoustic cavity ($L_x \times L_y \times L_z = 0.2032$ m $\times$ 0.4064 m $\times$ 0.6096 m) is coupled to a simply supported rectangular plate ($L_x \times L_y = 0.2032$ m $\times$ 0.4064 m) of thickness 1.524 mm. The other five walls of the cavity are considered as acoustically rigid. The material properties of the plate are specified as: Poisson's ratio $\mu = 0.3$, Young's modulus $E = 71 \times 10^9$ Pa and mass density $\rho_{panel} = 2700$ kg/m^3. The density of and sound speed in the air cavity are $\rho_{air} = 1.21$ kg/m^3 and $c_0 = 344$ m/s, respectively. In the current solution method, the simply supported boundary condition can be easily realized by respectively setting the stiffnesses of the rotational and translational springs to zero and infinity which is actually represented by a very large number, 5×10^9, in the numerical calculations.

Table 2 shows the first 20 natural frequencies of the coupled panel-cavity system. The data from Ref. [17] were also listed there for comparison. A nice agreement can be observed between these two sets of results with the largest difference being less than 0.35%. In this example, the Fourier series is truncated to $M_p = N_p = 12$ for plate displacement and to $M_{xa} = M_{ya} = M_{za} = 3$ for the cavity pressure.

Mode order	Ref. [17] (Hz)	Current (Hz)	Difference (%)
1	113.91	114.06	0.13
2	177.48	178.04	0.32
3	280.71	281.02	0.11
4	295.97	296.62	0.22
5	379.77	379.71	0.02
6	423.05	423.11	0.01
7	447.32	447.96	0.14
8	448.06	449.21	0.26
9	511.5	511.52	0.00
10	559.9	561.49	0.28
11	565.89	565.9	0.00
12	650.43	652.6	0.33
13	706.59	706.6	0.00
14	717.41	719.91	0.35
15	829.09	826.97	0.26
16	846.99	847	0.00
17	847.03	847.04	0.00
18	850.95	850.59	0.04
19	892.84	892.92	0.01
20	893.4	893.39	0.00

Table 2. The first 20 modal frequencies for the coupled panel-cavity system.

Next, we will examine the effect of cavity depth on the modal parameters. As in Ref. [18], the cavity dimensions are chosen as: $L_x \times L_y \times L_z = 0.2\ \text{m} \times 0.2\ \text{m} \times H_{depth}$. The cavity is enclosed at $z = L_z$ by a simply supported copper panel, and its remaining five walls are assumed to be perfectly rigid. The panel thickness is 0.9144 mm, and its material properties are mass density $\rho_s = 8440\ \text{kg/m}^3$, Poisson's ratio $\mu = 0.35$ and Young's modulus $E = 105 \times 10^9$ Pa. The acoustic medium is air having the same properties as in the first example. **Table 2** gives the first six modal frequencies of the coupled system with a good comparison with the results previously presented in Ref. [18].

From the standpoint of structural vibration, the acoustic cavity may be approximately viewed as Winkler springs with a probably non-uniform stiffness distribution over the area of the panel, depending upon frequency. To understand its significance, the effects of varying edge restraining stiffnesses on the fundamental frequency of the coupled system are studied for a range of cavity depths. In this analysis, the copper panel is assumed to be uniformly supported along all four edges. Shown in **Figure 7(a)** are the results for a configuration in which, by keeping the rotational stiffness to zero, the stiffness for the translational spring is increased from zero (completely free) to infinity (simply supported). It is evident that reducing the cavity

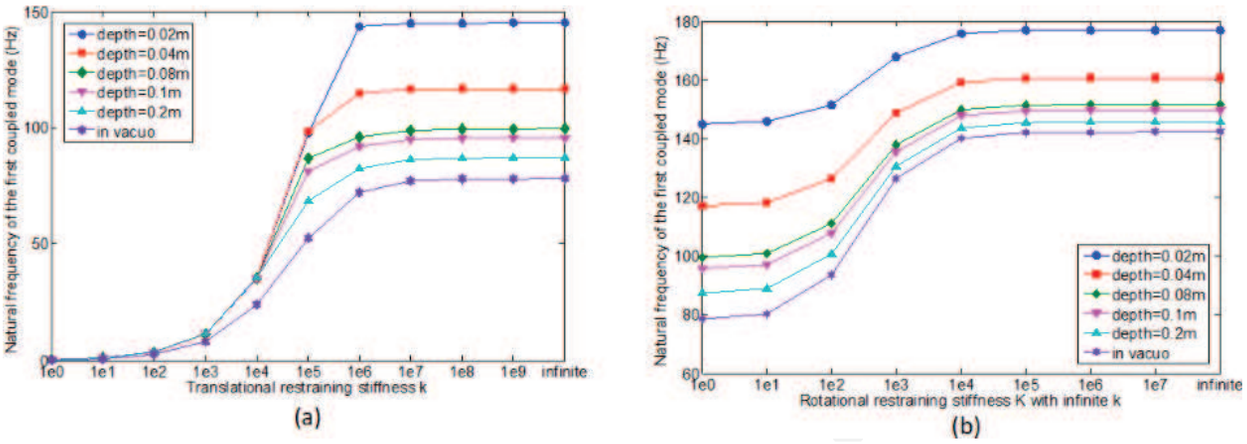


Figure 7. Effect of the boundary restraining stiffness on the first modal frequency of the coupled system: (a) varying the stiffness of the translational springs; (b) varying the rotational stiffness.

depth is equivalent to increasing the stiffness of the Winker springs. For small restraining stiffness, $k \leq 10^3$, the first mode is manifested in a piston-like motion, and the fundamental frequency is primarily determined by the edge restraints. However, as the edge springs become sufficiently strong, $k \geq 10^7$, the air cavity starts to take over as a dominating factor in affecting the value of the fundamental frequency. For intermediate values, $10^4 \leq k \leq 10^6$, the fundamental frequency tends to show a strong dependence on the stiffness of the edge restraints.

By letting the translational springs be infinitely rigid, we now add rotational restraints to the edges. The fundamental frequency curves are plotted in **Figure 7(b)** for various combinations of cavity depths and spring stiffnesses. Again, it is seen that the decreasing the cavity depth is equivalent to increasing the stiffness of the Winkler springs and hence the fundamental frequency of the panel wall. The above results also indicate that there tends to exist stronger structural acoustic coupling for a thinner air gap. This statement may have a meaningful implication to the design of double-walled sound isolation.

We will now direct our attention to the vibro-acoustic responses of the coupled system. For validation, the cavity dimensions will be modified to: $L_x \times L_y \times L_z = 1.5\ \text{m} \times 0.3\ \text{m} \times 0.4\ \text{m}$. The top surface of the cavity is a simply supported plate of thickness $h = 5$ mm. Other relevant material properties are given as: $\rho_{\text{Al}} = 2770\ \text{kg/m}^3$, Young's modulus $E = 71 \times 10^9$ Pa, Poisson's ratio $\mu = 0.33$, air density $\rho_{\text{air}} = 1.21\ \text{kg/m}^3$ and speed of sound $v = 340$ m/s. The damping ratio $\xi = 0.01$ is used for both the plate and air cavities. A unit force is applied to the plate at point $(13L_x/30, L_y/2)$. This model was studied before by Kim and Brennan [19] using an impedance and mobility approach which is essentially the same as the modal coupling theory. **Figure 8** shows the velocity responses at two separate locations, $(13L_x/30, L_y/2)$ and $(16L_x/30, L_y/3)$. Plotted in **Figure 9** are the sound pressures inside the cavity at $(4L_x/10, L_y/2, L_z/2)$ and $(L_x/2, L_y/2, L_z/2)$. The reference values in the dB scales are 10^{-9} m/s for velocity and 2×10^{-5} Pa for sound pressure. It is seen that both the resonant peaks (namely, natural frequencies of the coupled system) and magnitude of the calculated vibrational and acoustic responses match very well with the analytical predictions from the impedance and mobility approach [19],

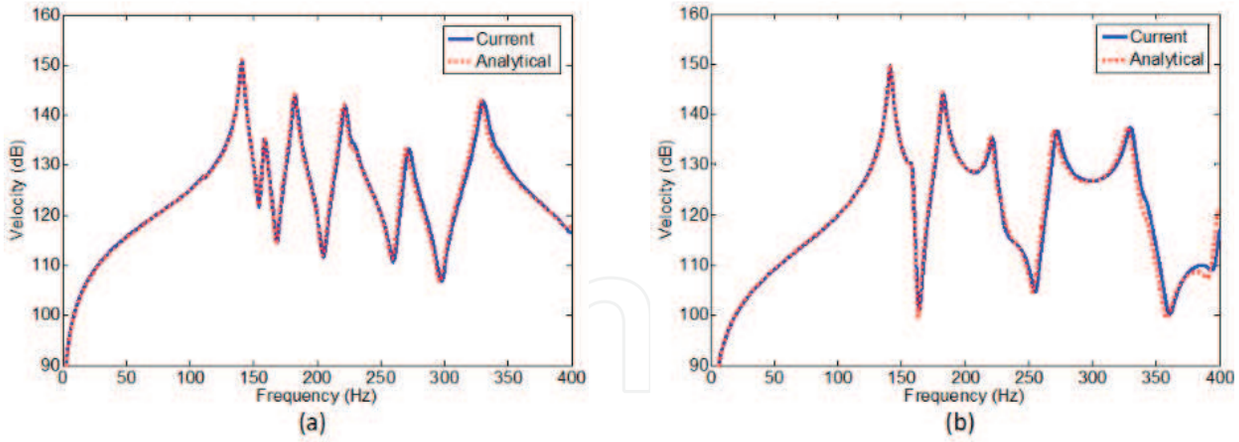


Figure 8. Velocity responses of the plate at: (a) ($13L_x/30$, $L_y/2$) and (b) ($16L_x/30$, $L_y/3$).

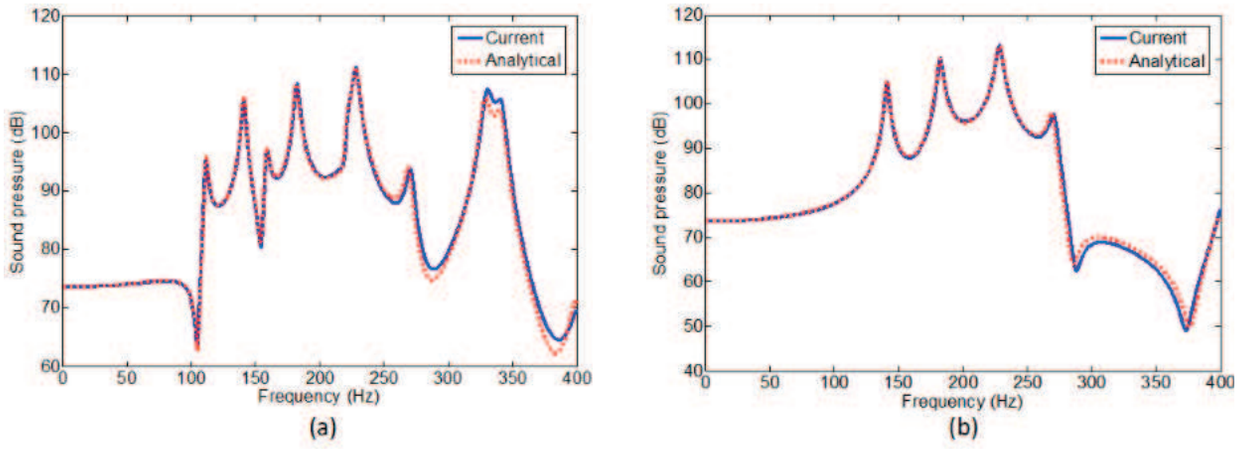


Figure 9. Sound pressure responses at: (a) ($4L_x/10$, $L_y/2$, $L_z/2$) and (b) ($L_x/2$, $L_y/2$, $L_z/2$).

which are plotted as the dotted curves in **Figures 8** and **9**. In this analysis, the Fourier series is truncated to $M_p = N_p = 12$ for the plate displacement and to $M_{xa} = 5$, $M_{ya} = M_{za} = 3$ for the cavity pressure.

As mentioned earlier, the conventional modal coupling theory suffers a velocity discontinuity problem at the fluid-structure interface, that is, the particle velocity on/near the interface cannot correctly calculated from the pressure gradient. However, this velocity continuity requirement is faithfully enforced in the current method. To illustrate this point, **Figure 10(a)** shows the velocity response at ($3L_x/10$, $L_y/4$, L_z) on the panel. Because of the relatively large length-to-width ratio ($L_x/L_y = 1.5/0.3 = 5$), it is reasonable to include more x-related terms in the Fourier series for the cavity pressure to better capture the faster variation of pressure gradient in the x-direction. It is seen that setting the truncation number to $M_x = 10$ has effectively ensured the velocity continuity on the interface. The direct and indirect velocities are also compared in **Figure 10(b)** at a different point, ($L_x/4$, $L_y/4$, L_z), on the interface. Plotted in **Figure 11** are the comparisons of the velocity responses at ($3L_x/10$, $4L_y/5$, z) predicted by the

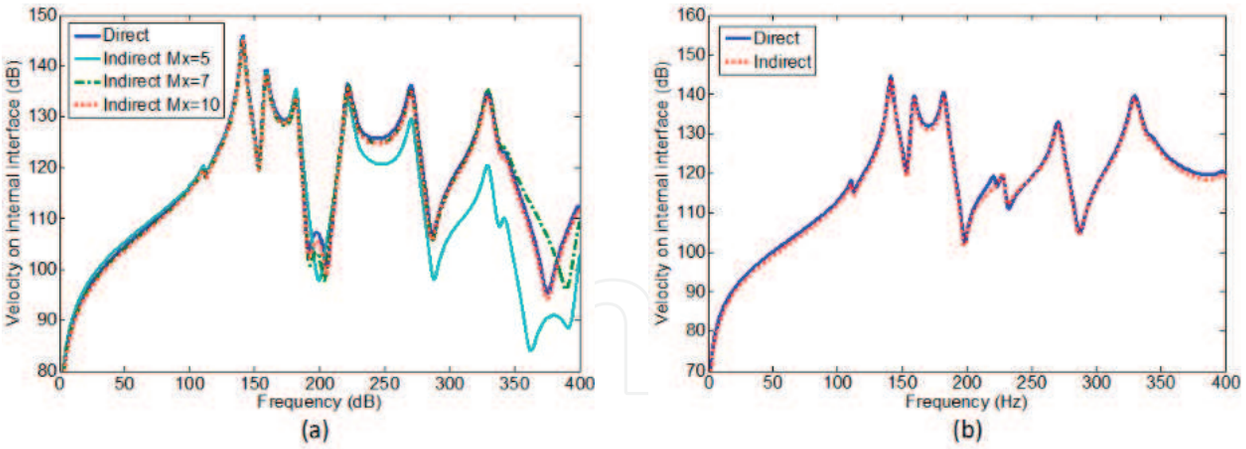


Figure 10. Velocity responses on the interface at: (a) ($3L_x/10$, $L_y/4$) and (b) ($L_x/4$, $L_y/4$).

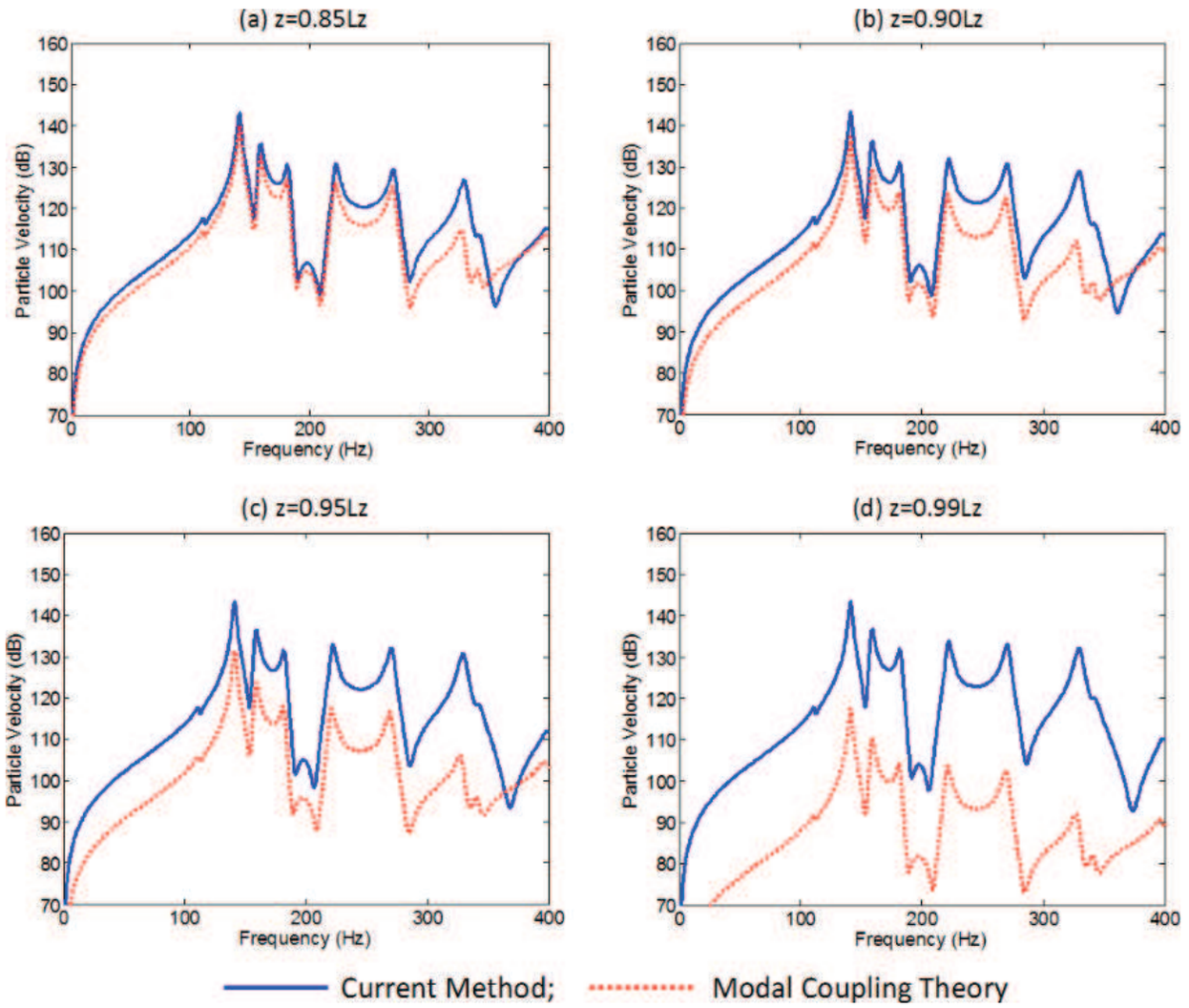


Figure 11. Comparison of the current method and modal coupling theory on predicting the particle velocity response at ($3L_x/10$, $4L_y/5$, z) with different spatial coordinates along z-axis: (a) $z = 0.85L_z$; (b) $z = 0.90L_z$; (c) $z = 0.95L_z$; and (d) $z = 0.99L_z$.

http://dx.doi.org/10.5772/intechopen.69967

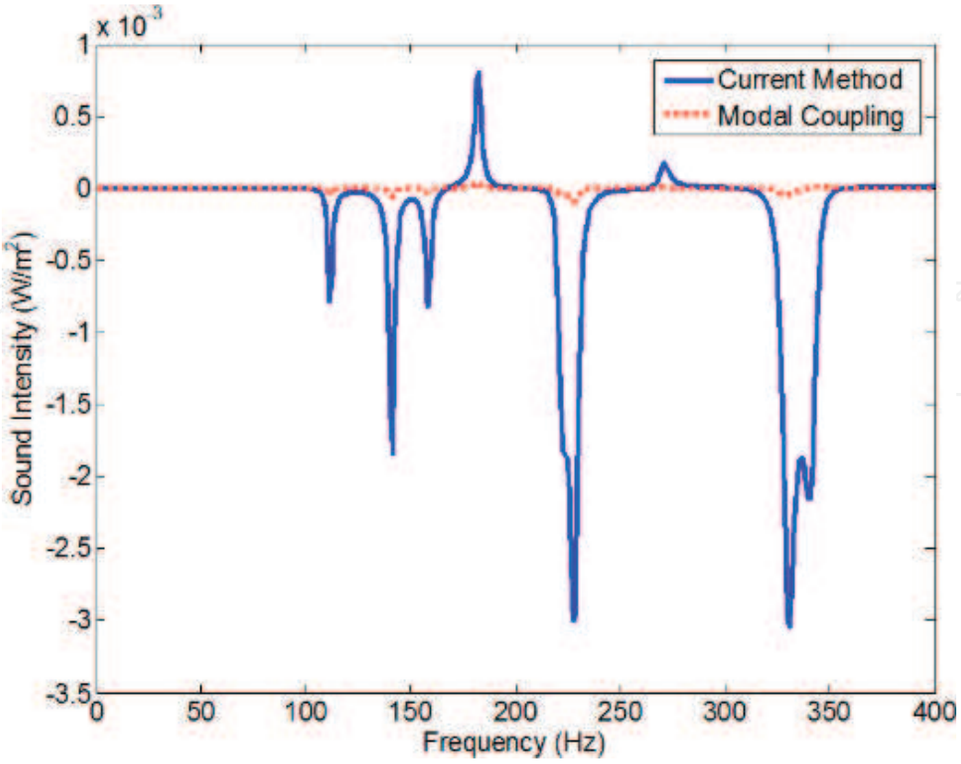


Figure 12. Sound intensity at ($3L_x/10$, $4L_y/5$, $0.99L_z$) predicted by current method and modal coupling theory.

current method and modal coupling theory for different z-values: $z = 0.85L_z$, $0.90L_z$, $0.95L_z$ and $0.99L_z$. It is observed that the particle velocity can be better estimated by using the current method, particularly for the cases very close to the panel-cavity interface. Once the reliable prediction has been made for the particle velocity, other variables of interest such as sound intensity can be calculated. **Figure 12** presents the calculated sound intensity near the interface at ($3L_x/10$, $4L_y/5$, $0.99L_z$). Since sound intensity is a vector, the negative value indicates that its direction is opposite to the z-axis. It can be found that the acoustic energy is not always transmitted from the vibrating panel into acoustical cavity in the whole frequency range at this observing point. The calculated results using modal coupling theory are also shown there; obviously, such an approach cannot be correctly used to predict sound intensity due to its poor accuracy with predicting particle velocity from pressure gradient in the vicinity of the vibrating boundary structure.

4. Conclusions

An improved Fourier series method is presented for the acoustic/vibro-acoustic modelling of acoustic cavity as well as its coupling with flexible boundary structure. The coupled system is described in a unified pattern by using the energy description. With the aim to construct the structural-acoustic admissible functions smooth sufficiently in the whole solving domain, boundary-smoothed auxiliary functions are introduced to the standard multi-dimensional Fourier series on the system boundary as well as the coupling interface. In conjunction with

Rayleigh-Ritz procedure, all the unknown coefficients can be easily derived, and the relevant higher order acoustic variables, such as energy power flow, can be determined straightforwardly.

The theoretical formulation is implemented in the Matlab environment. Numerical results are presented to illustrate the effectiveness and efficiency of the proposed model. The correctness and reliability is then verified by comparing with those from other method or numerical solution. Based on the model established, influence of boundary condition on the acoustic or structural-acoustic coupling characteristics is addressed and investigated in details. This work can present an efficient analysis tool for the acoustic or structural-acoustic analysis of the enclosed sound space and flexible structure. This work shows that the desired modal characteristics of coupling system can be obtained by adjusting boundary conditions properly.

Acknowledgements

This work was supported by the Fundamental Research Funds for the Central Universities (HEUCFP201758).

Author details

Jingtao Du*, Yang Liu and Long Liu

*Address all correspondence to: dujingtao@hrbeu.edu.cn

College of Power and Energy Engineering, Harbin Engineering University, Harbin, PR China

References

[1] Kelsall G, Troger C. Prediction and control of combustion instabilities in industrial gas turbines. Applied Thermal Engineering. 2004;**24**:1571-1582. DOI: 10.1016/j.applthermaleng.2003.10.025

[2] Morse PM, Bolt RH. Sound waves in rooms. Reviews of Modern Physics. 1944;**16**:69-150. DOI: 10.1103/RevModPhys.16.69

[3] Maa DY. Non-uniform acoustical boundaries in rectangular rooms. Journal of the Acoustical Society of America. 1940;**12**:39-52. DOI: 10.1121/1.1916070

[4] Bistafa SR, Morrissey JW. Numerical solutions of the acoustic eigenvalue equation in the rectangular room with arbitrary (uniform) wall impedances. Journal of Sound and Vibration. 2003;**263**:205-218. DOI: 10.1016/S0022-460X(02)01123-9

[5] Naka Y, Oberai AA, Shinn-Cunningham BG. Acoustic eigenvalues of rectangular rooms with arbitrary wall impedances using the interval Newton/generalized bisection method. Journal of the Acoustical Society of America. 2005;**118**:3662-3671. DOI: 10.1121/1.2114607

[6] Fahy FJ. Sound and Structural Vibration: Radiation, Transmission and Response. New York: Academic; 1985

[7] Pan J, Bies DA. The effect of fluid-structural coupling on sound waves in an enclosure, theoretical part. Journal of the Acoustical Society of America. 1990;**87**(2):691-707. DOI: 10.1121/1.398939

[8] Pan J, Hansen CH, Bies DA. Active control of noise transmission through a panel into a cavity: I. Analytical study. Journal of the Acoustical Society of America. 1990;**87**:2098-2108. DOI: 10.1121/1.399555

[9] Du JT, Li WL, Liu ZG, Xu HA, Ji ZL. Acoustic analysis of a rectangular cavity with general impedance boundary conditions. Journal of the Acoustical Society of America. 2011;**130**(2):807-817. DOI: 10.1121/1.3605534

[10] Du JT, Li WL, Jin GY, Yang TJ, Liu ZG. An analytical method for the in-plane vibration analysis of rectangular plates with elastically restrained edges. Journal of Sound and Vibration. 2007;**306**:908-927. DOI: 10.1016/j.jsv.2007.06.011

[11] Li WL. Comparison of Fourier sine and cosine series expansions for beams with arbitrary boundary conditions. Journal of Sound and Vibration. 2002;**255**:185-194. DOI: 10.1006/jsvi.2001.4108

[12] Crighton DG, Dowling AP, Ffowcs Williams JE, Heckl M, Leppington FG. Modern Methods in Analytical Acoustics. Berlin: Springer-Verlag; 1992

[13] Ginsberg JH. Mechanical and Structural Vibrations: Theory and Applications. New York, John Wiley & Sons; 2001

[14] Li WL, Zhang XF, Du JT, Liu ZG. An exact series solution for the transverse vibration of rectangular plates with general elastic boundary supports. Journal of Sound and Vibration. 2009;**321**:254-269. DOI: 10.1016/j.jsv.2008.09.035

[15] Du JT, Li WL, Xu HA, Liu ZG. Vibro-acoustic analysis of a rectangular cavity bounded by a flexible panel with elastically restrained edges. Journal of the Acoustical Society of America. 2012;**131**(4):2799-2810. DOI: 10.1121/1.3693652

[16] Johnson ME, Elliott SJ, Beak K-H, Garcia-Bonito J. An equivalent source technique for calculating the sound field inside an enclosure containing scattering objects. Journal of the Acoustical Society of America. 1998;**104**:1221-1231. DOI: 10.1121/1.424330

[17] Rajalingham C, Bhat RB, Xistris GD. Natural vibration of a cavity backed rectangular plate using a receptor-rejector system. Journal of Vibration and Acoustics. 1995;**117**: 416-423. DOI: 10.1115/1.2874473

[18] Guy RW. Pressure developed within a cavity backing a finite panel when subjected to external transient excitation. Journal of the Acoustical Society of America. 1980;**68**: 1736-1747. DOI: 10.1115/1.2874473

[19] Kim SM, Brennan MJ. A compact matrix formulation using the impedance and mobility approach for the analysis of structural-acoustic systems. Journal of Vibration and Acoustics. 1999;**223**(1):97-113. DOI: 10.1006/jsvi.1998.2096

IntechOpen

IntechOpen